Harnessing sleep/wake state tracking by olfactory bulb oscillations to perform fully brain-based sleep scoring in mice

Sophie Bagur[1], Marie Masako Lacroix[1], Gaëtan de Lavilléon[1], Julie M Lefort[1], Hélène Geoffroy[1], Karim Benchenane[1]

[1]*Team Memory, Oscillations and Brain States (MOBs), Brain Plasticity Unit, CNRS, ESPCI Paris, PSL Research University, 10 rue Vauquelin, Paris, France.*

Abstract

There is growing interest in sleep research and finding easily tracked neural correlates of brain states is a central challenge to the definition of sleep and wake states. Here we demonstrate using multi-site electrophysiological LFP recordings in freely moving mice that gamma power in the olfactory bulb (OB) allows for clear classification of sleep and wake. Coupled with hippocampal theta activity, it allows the construction of a robust and reproducible sleep scoring algorithm that relies on brain activity alone. We validate the procedure by comparison with classical methods based on muscular activity (EMG) and video tracking. Contrary to EMG, OB gamma power allows correct discrimination between sleep and immobility in ambiguous situations such as fear-related freezing. Finally, beta power in the OB is a good predictor of Rapid Eye Movement sleep. Overall, our results reveal the OB can be used as a highly reliable readout of brain states.

Introduction

A current challenge in neuroscience is defining the different states of brain activity and describing how they impact the computations performed by neural networks. The most dramatic change of state is that between sleep and wakefulness that involves modifications of cortical activation (Steriade *et al.*, 1993), gene expression (Cirelli & Tononi, 2000), engagement with the outside world and clearance mechanisms (Xie *et al.*, 2013) amongst other changes throughout the whole organism (Benington & Heller, 1995; Imeri & Opp, 2009). Despite these profound transformations, to date, we surprisingly lack an easily measured marker of brain activity that allows unambiguous, moment-to-moment identification of sleep and wake states.

Several sleep scoring methods have been proposed in human research (Rechtschaffen & Kales, 1968; Iber *et al.*, 2007) and are now widely accepted by the scientific community. Sleep scoring procedures in the rodent on the contrary remain less uniformly adopted (Datta & Hobson, 2000) and often vary from laboratory to laboratory. Moreover all current sleep scoring methods essentially rely on motor activity to discriminate sleep from wake, see Table 1 (Veasey *et al.*, 2000; Louis *et al.*, 2004; Crisler *et al.*, 2008; Gross *et al.*, 2009; Stephenson *et al.*, 2009; Brankack *et al.*, 2010; Rytkönen *et al.*, 2011; Liang *et al.*, 2012; Zeng *et al.*, 2012).

Most methods of sleep scoring are either completely manual or rely on manually scored training data to calibrate automatic algorithms (Table 1). This time-consuming approach is subject to inter-scorer variability. Moreover, these methods are inherently vulnerable to any mismatch between these brain states and the level of motor activity such as during freezing, a commonly-used behaviour in mice or any sleep anomalies causing movement during sleep (Schenck & Mahowald, 2002).

The state of the art therefore presents both a conceptual and a technical problem regarding the definition of sleep and wake.

Several attempts have been made to identify sleep with brain signals only. Generally, these procedures rely on more elaborate methods that extract composite features from LFP data (Gervasoni *et al.*, 2004). The main problem of this approach is that it relies entirely on the available data. The resulting axes onto which the data are projected vary from animal to animal and therefore always require post-hoc human labelling procedures. Moreover, this makes the resulting state maps only qualitatively comparable between animals (Gervasoni *et al.*, 2004). Finally, these maps can be used to describe sleep states but it is generally impossible to use them for sleep scoring because of the low separation between states (Gervasoni *et al.*, 2004).

Sleep scoring methods are based on the assumption that the information about sleep states is contained in the recorded signal and can be used as a marker (Libourel *et al.*, 2015). In order to implement a reliable sleep scoring, the candidate marker of sleep and wake must not only show a strong average difference between the two states but this change must be systematic and sustained throughout each state, with a clear separation between the values in each state. A bimodal distribution with good separation of the two component distributions is the optimal situation to allow moment-by-moment discrimination.

Despite multiple attempts, such a clear-cut situation has never been found when using brain signals (Brankack *et al.*, 2010). To compensate for the poor quality of the brain-related sleep markers, machine learning techniques have been used in several studies but with no decisive improvement (Crisler *et al.*, 2008; Yu *et al.*, 2009; Rytkönen *et al.*, 2011; Chou *et al.*, 2013). Here we propose a novel brain-related marker allowing to reliably track transitions from sleep to wakefulness. Indeed the gamma power (50-70Hz) measured in the olfactory bulb has been shown to vary between sleep states (Manabe & Mori, 2013) but we show here that it displays the desired characteristics to continuously identify the different sleep states. Interestingly, the olfactory bulb receives massive projections from the main neuromodulator systems involved in the control of sleep stages (Wenk *et al.*, 1980; Shipley *et al.*, 1985; Senut *et al.*, 1989; Gascuel *et al.*, 2012). In turn, the different neuromodulators have been shown to modulate gamma oscillations (Hall & Delaney, 2001; Gire & Schoppa, 2008; Li & Cleland, 2013). We thus propose that these oscillations can be used as a direct read-out of the brain network responsible for sleep/wakefulness cycles. Accordingly, we show that the gamma oscillation in the olfactory bulb is strongly suppressed during sleep and continuously present during waking. Moreover, the distribution of the gamma power follows a bimodal distribution that is the optimal situation for an automatic separation procedure. Coupling this indicator with the classical hippocampal theta/delta power ratio allows us to construct a fully automated sleep scoring algorithm that classifies wake, rapid eye movement sleep (REM) and non-REM sleep (NREM) based on brain state alone. We then use these variables to construct a robust 2D phase-space that is highly robust across mice and days. We can therefore easily compare the dynamics of transitions between sleep and wake states across animals. Together, we propose a new sleep scoring method that has strong methodological (automatic, reproducible, no training data required) and conceptual (no reliance on motor activity) advantages over traditional methods.

Results

Olfactory bulb gamma power modulation throughout brain states

Classical sleep scoring methods differentiate sleep and wake states using EMG activity or the animal's motion recorded using accelerometers or video tracking (see Table 1, Veasey *et al.*, 2000; Louis *et al.*, 2004; Crisler *et al.*, 2008; Gross *et al.*, 2009; Stephenson *et al.*, 2009; Brankack *et al.*, 2010; Rytkönen *et al.*, 2011; Liang *et al.*, 2012; Zeng *et al.*, 2012). Theta and delta power recorded in the hippocampus or cortex (due to the volume conduction of theta oscillations) can

then be used to discriminate REM from NREM sleep. According to classical sleep scoring methods, wake is defined by high EMG activity and low HPC signal during arousals, irregular HPC activity during quiet wake or theta oscillation during active exploration. On the contrary, sleep is defined by low EMG power and NREM is discriminated from REM using the theta/delta power ratio in the hippocampus. During NREM delta power is strong whereas highly regular theta oscillations are observed during REM (Figure 1A).

Citation	Motor params.	Brain activity params.	Manual calibration
Brankack et al., 2010	EMG	EEG power : delta (1–4 Hz), theta2 (7–8.5 Hz) and gamma2 (52– 70 Hz)	Training data (5%) for LDA or classification tree
Crisler et al., 2008	EMG	EEG :107 temporal and spectral parameters	Training data (2 hours of recording) for SVM
Gross et al., 2009	EMG	EEG : Delta, theta, sigma and beta bands	Training data and manual determination of thresholds
Louis et al., 2004	EMG	EEG : Delta, theta , alpha, beta and gamma	Training data for threshold determination (1 day recording)
Rytkönen et al., 2011	EMG	EEG : Delta, theta , alpha, beta and gamma	Training data (5%) for naïve Bayes classifier
Veasey et al., 2000	EMG	EEG : Delta, sigma , theta	Visual determination of thresholds
Zeng et al., 2012	Doppler and video recording of movement and breathing	none	Training data for SVM
Liang et al., 2012	EMG	13 EEG features	Training on 2 animals for all other animals to tune parameters
Stephenson et al., 2009	EMG	EEG : delta, alpha, theta, beta and gamma power	No manual steps

Table 1

In order to construct a sleep scoring method that relies on brain signals alone, we screened multiple brain regions to find a good predictor for discriminating between sleep and waking states. We recorded from multiple brain regions in 15 freely-moving mice: the olfactory bulb (OB, n=15), the hippocampus (HPC, n=15), the prefrontal cortex (PFCx, n=6) and the parietal cortex (PaCx, n=6) cortex. Mice were recorded for an average of 6.6 ± 0.58 hrs (minimal recording length : 2hrs) in their homecages in the light period and slept on average 58% of the time. We initially used a classical sleep scoring method based on movement and hippocampal activity to establish a database of recordings from different brain states using 10 of the 15 mice that either were implanted with an EMG wire in the nuchal muscles (n=6) or tracked using video (n=4).

The average spectra over wake, NREM and REM periods are shown in figure 1B. In cortical and hippocampal areas, as expected, REM and NREM showed strong differences in the theta and delta band and wake periods showed less low frequency power. In cortical and hippocampal areas, no individual frequency band allows to discriminate well between sleep and wake. Linear combinations of these parameters extracted using PCA have been show to display some clustering of brain states but is not sufficient for a reliable identification of sleep states on its own (Gervasoni *et al.*, 2004).

Remarkably however, we found a strong increase in power in the OB during waking relative to sleep states. This difference was strongest in the low gamma band centred at 60Hz as previously described (Manabe & Mori, 2013). This change is clear in the figure 1A which shows OB activity that is constantly modulated by the breathing cycle but which displays a sustained faster oscillation only in the wake state. Crucially, gamma power was low in both sleep states, suggesting that this parameter could replace muscle activity for discriminating wake from REM sleep.

However, when using gamma power in the OB to identify brain states, we face the problem that it displays strong fluctuations correlated with breathing activity on the scale of around a second (Manabe & Mori, 2013). To find the appropriate time scale for tracking the changes in gamma power related to brain state changes, we applied a smoothing window of varying length to the instantaneous gamma power. As the smoothing window increased in length, the distribution of gamma power became more distinctly bimodal and the two underlying distributions clearly separated (Figure 1C-D). We found that smoothing windows larger than 1s produced two normal distributions overlapped by less than 5% (Figure 1D bottom). This analysis allowed us to establish a set of parameters (frequency, smoothing window) that establish gamma power in the OB as a promising predictor for discriminating between wake and sleep on fine timescales of the order of one second without any reliance on muscular activity.

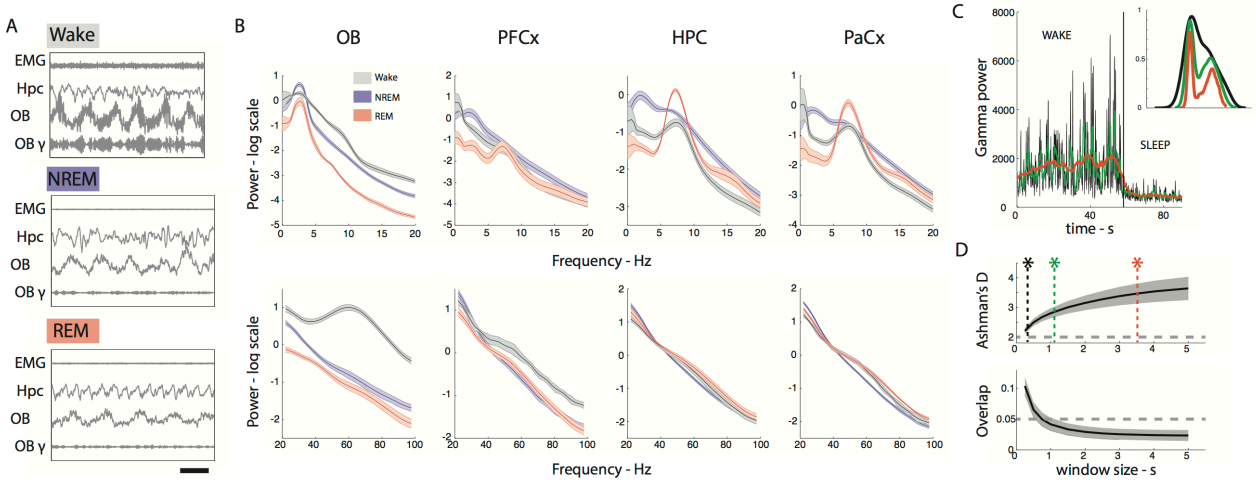

Figure 1

A. *Example data showing EMG, HPC and OB activity in three brain states. Wake is characterized by high EMG activity and high gamma power in the OB whereas sleep is characterized by low EMG activity and low gamma power in the OB. HPC LFP shows regular theta activity during REM sleep. Filtered signals from the OB in the gamma band (OB-γ, 50-70Hz) shows the remarkable decrease in gamma during sleep states. (Scale bar : 0.5s)*

B. *Low (top) and high (bottom) frequency spectra from different brain regions during NREM, REM and wake states as classified using movement based scoring (EMG or filmed activity). Note the strong increase in gamma activity in the OB in the wake state. (n=10 for OB and HPC, n=6 for PFCx and PaCx, error bars : s.e.m)*

C. *Gamma power in OB is plotted as a function of time as the animal transitions from wake to sleep and the distribution of the corresponding values is shown on the right. The data has been smoothed different window lengths (0.1, 1 and 4s respectively). The fast fluctuations present in the awake state are smoothed out as the window size increases yielding a more clearly bimodal distribution with larger smoothing window.*

D. *Ashman's D (bimodality indicator, significant if larger than 2) (i) increases and the overlap between the two gaussians (ii) decreases with the length of the smoothing window. The stars show window sizes illustrated in C.*

Construction of the sleep scoring algorithm

A schematic of the sleep scoring algorithm is shown in figure 2A. All steps are automatic and do not require any supervision by the user. Instantaneous smoothed gamma power in the OB shows a bimodal distribution that can be well fit by a sum of two gaussian functions (Figure 2B) (mean R^2 =0.98 ± 0.009). The two component distributions correspond to gamma power during sleep and wake periods defined by movement. Since the amplitude of these distributions depends on the proportion of time spent in each state, they are normalized (see Methods) and the sleep/wake threshold is defined as the intersection of the two Gaussian curves (Figure 2Bi). Below threshold values of gamma power are defined as sleep and above threshold values as wake.

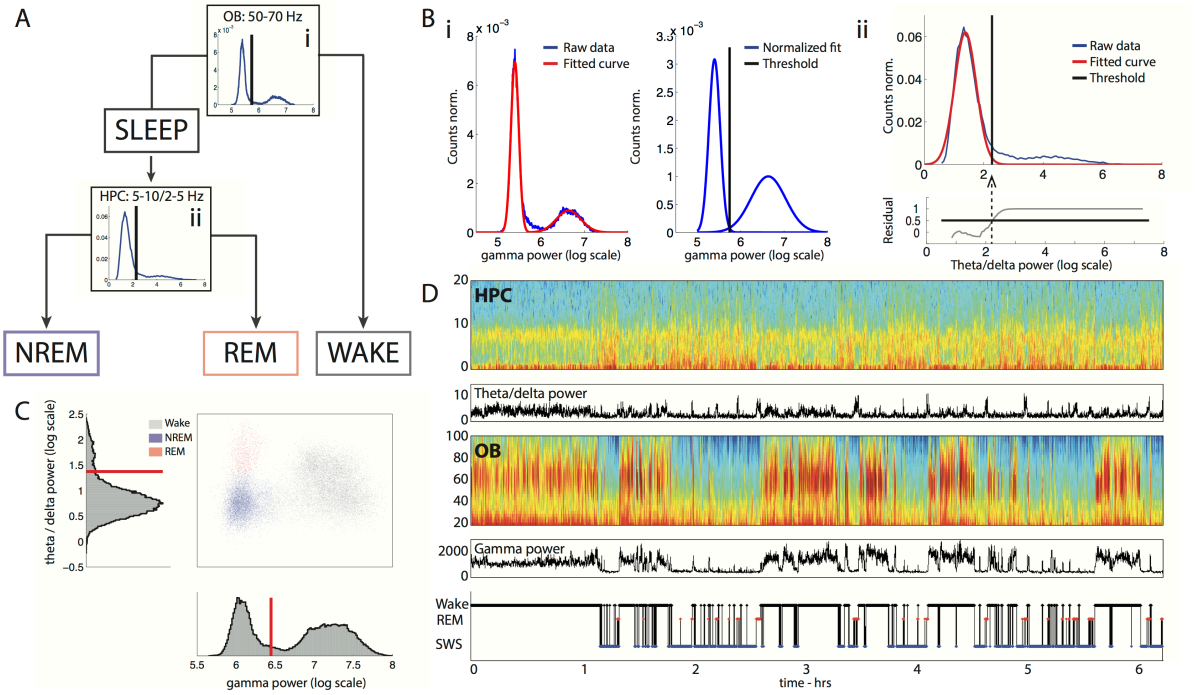

Figure 2

A . *Flowchart of data through the scoring algorithm. Sleep and wake states are first classified based on OB gamma (i). Sleep data is then further classified into REM and NREM based on HPC theta / delta power ratio (ii).*

B. *Example of automatic thresholding of distributions.*

(i) Two gaussian distributions are fit to the distribution of OB gamma power (left) and their areas are equalized (right). The threshold is placed at the intersection of the two distributions.

(ii) A gaussian distribution is fitted to the distribution of HPC theta / delta power ratio during sleep. The residuals are shown in the bottom plot. The threshold is placed at the point where the fit explains less than 50% of the data.

C. *Example 2D phase space. Each 3s period of recording is plotted according to its average OB gamma power value and average HPC theta / delta power ratio showing the three brain states identified: NREM (blue), REM (red) and Wake (grey). Corresponding histograms are shown along the relevant axis with automatically determined thresholds in red.*

D. *Example data set showing HPC low frequency spectrogram (i) with theta / delta power ratio below and OB high frequency spectrogram (iii) with gamma power below. Hypnogram is shown at the bottom.*

The instantaneous smoothed theta/delta power ratio in the HPC LFP is used to discriminate NREM from REM sleep as in classical sleep scoring. When restricting this variable to the sleep period only, it shows a peak and slab type distribution. The spike is well fit by a Gaussian (mean R^2: 0.97 ± 0.004) corresponding to the NREM period and the slab contains the values from the REM period. The threshold separating REM and NREM sleep is defined as the value above which the residuals of the Gaussian fit explain more than 50% of the data (Figure 2Bii). Importantly, the distribution of theta/delta power ratio during both sleep and wake states does not allow to define a natural threshold and so the two steps of the algorithm must be performed in this order.

Each time point is now attributed to one of the three states, based on its OB gamma power and HPC theta/delta ratio (Figure 2C). Brief periods of less than 3s are merged with the neighbour states (see methods for details). An example session is shown in figures 2C-D that illustrates the construction of a two dimensional phase space for brain states (Figure 2C). This space demonstrates the clear separation of brain states even after the merging and dropping of short epochs. This suggests that the continuity hypothesis does not lead to any aberrant classification.

Validation of the sleep scoring algorithm

We validated the sleep scoring algorithm by comparing it to manual sleep scoring performed using HPC LFPs and EMG activity, the classical golden standard. Two expert scorers independently scored sessions from 4 mice with an average inter-scorer overlap of 89 ± 3% and Cohen's K of 0.81. On average the automatic and manual sleep scoring overlapped by 90 ± 2% (Cohen's K : 0.83) throughout the sessions (Figure 3A).

To more systematically compare the two approaches used to distinguish wake from sleep, gamma power in the OB and EMG power, we also performed scoring using an automatic EMG scoring algorithm (see Methods). Agreement between the two approaches was 93% (Cohen's K : 0.85) (Figure 3B) on average and the two signals were highly correlated at all times and time-locked at transition points (Figure 3C,D).

We compared how well the distributions of each variable were described by fitting with two Gaussians (Figure 3E). Both variables were strongly bimodal (Figure 3E, *left*), however the error of the fit is higher for the EMG power. We found that this error was explained by a higher proportion of values in the trough between the two Gaussians (11 ± 2% for EMG and 4 ± 3% for gamma power). This indicates that the 'ambiguous' zone between sleep and wake is more densely occupied when using EMG scoring leading to more potential errors.

This demonstrates that sleep scoring using gamma power in the OB and EMG, using either automatic or manual methods, give very similar classification of brain states, confirming that gamma power is a good predictor of wake and sleep as classically defined. Moreover, gamma power provides distributions with a clearer separation than EMG power, making it a more reliable predictor.

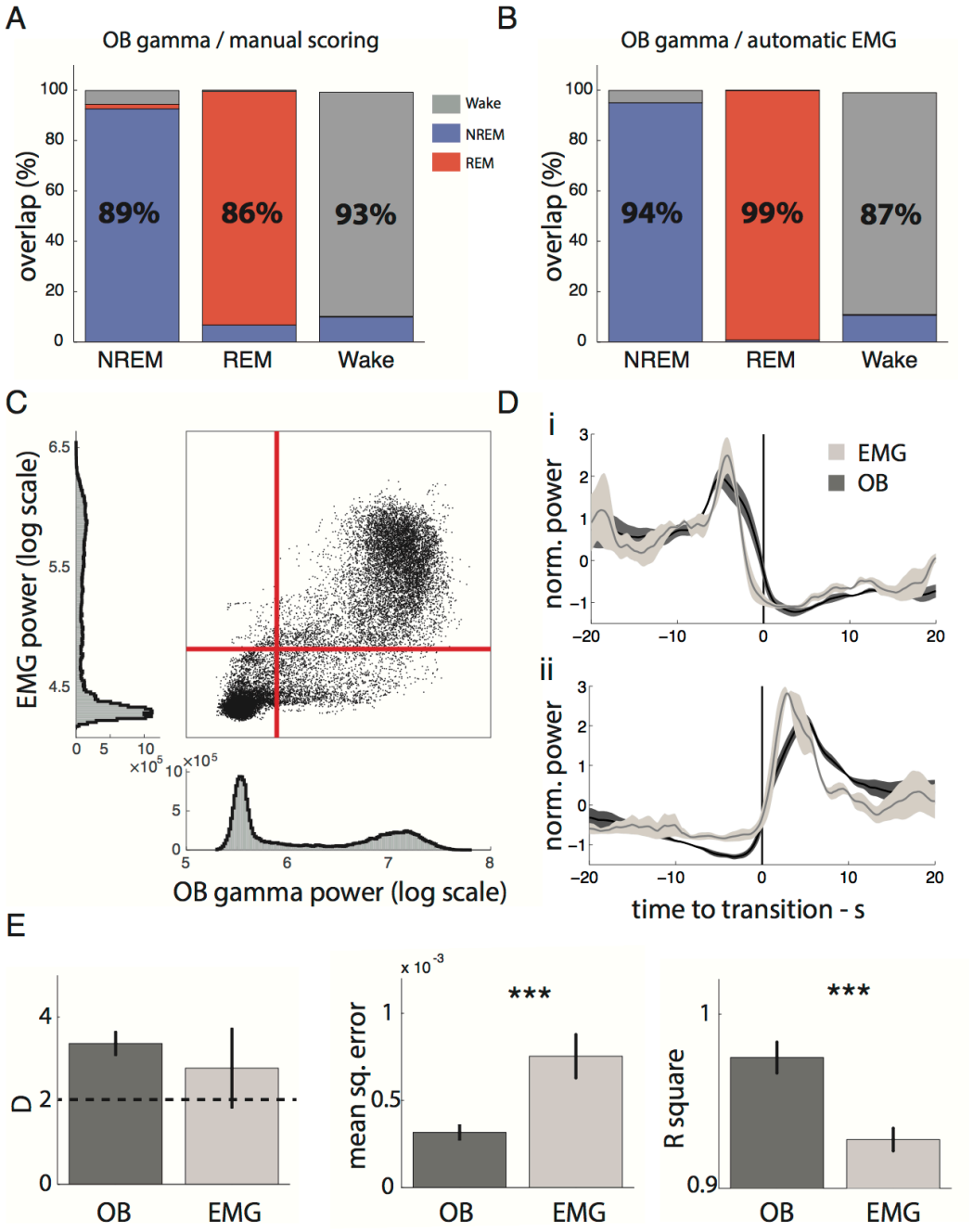

193

Figure 3

A. *Overlap of manual scoring with OB gamma scoring. Each column gives the percent of manually identified brain state (x label) that is classified as NREM (blue), REM (red) and wake (grey) respectively using OB gamma scoring. (n=6)*

B. *Overlap of automatic EMG scoring with OB gamma scoring. (n=6)*

C . *Correlation of OB gamma power and EMG power for an example mouse with automatically determined thresholds for each distribution in red. Dots in the upper right and lower left hand corner are identically classified by both approaches.*

D. *OB gamma and EMG power triggered on transitions from wake to sleep and sleep to wake determined by the OB gamma demonstrating tight temporal locking of changes with both indicators (n=6).*

E. *Comparison of the fit quality of bimodal distribution of two gaussians to gamma power and EMG power distributions. Both distributions are strongly bimodal as the average Ashman's D is larger than 2. However both mean square error and Rsquare show that gamma power distributions are better fit by a sum of gaussians. (n=15 for gamma, n=6 for EMG. Ttest,=p=0.43, 0.009,0.0005 respectively)*

194

Robustness of the sleep scoring method

Sleep scoring is often performed on large batches of animals, requiring simple surgeries and a high success rate. It is known that theta rhythm can be easily recorded in the hippocampal area using a single LFP wire. How does gamma power used for sleep scoring depend on the exact placement of the recording site? To answer this question, we simultaneously recorded activity from multiple depths in the olfactory bulb covering the outer and inner plexiform layers, the mitral cell layer and granular cell layer using a sixteen site linear probe (Figure 4A). We found that gamma oscillations could be observed at all depths and sleep scoring performed using electrodes at all depth highly overlapped (>92%) with classical, movement based sleep scoring (Figure 4B). We however observed that the separation between wake and sleep peaks was best in the deeper recording sites and in particular the most coherent scoring was found in those sites within the granule cell layer where gamma oscillations are visibly stronger (Figure 4C,D).

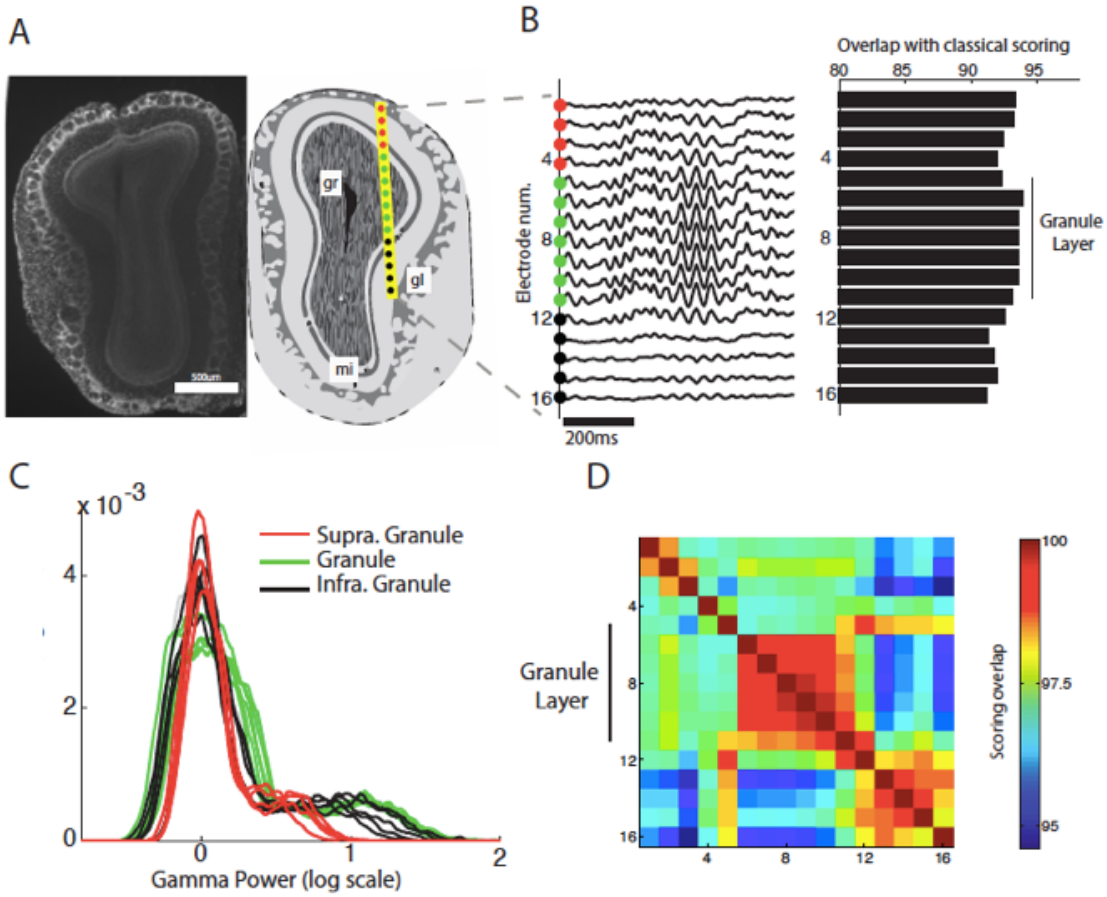

Figure 4

A. *Anatomical position (right) of 16-site silicon probe in the olfactory bulb as estimated from histological examination (left). This allows to estimate that sites 1-4 are above the granule layer and sites 12-16 are below.*

B. *Sleep scoring is performed using the gamma activity from each electrode site and compared to sleep scoring using the animal's movement. Accuracy is calculated as total overlap in sleep/wake periods.*

C. *Gamma power distributions for each electrode separated into supragranular, granular and infragranular layers. Note that the strong separation of sleep and wake peaks is clearest in electrodes within and below the granule layer.*

D. *Correlation matrix of sleep scoring performed using gamma power from different depths. Each square shows the percent overlap between scoring performed with the corresponding electrodes. All values are high (above 95%) but the granule cell layer shows particularly coherent scoring (>99%).*

This demonstrates that placement of the LFP wire for reliable scoring does not require great precision during implantation, assuring good scoring for all implanted animals. The granule cell layer however appears to be the optimal anatomical region to ensure reliable scoring since it shows the highest coherence in gamma power fluctuations. The coordinates we recommend aim for the center of this zone (AP +4, ML +0.5, DV −1.5).

An optimal sleep scoring technique must provide easily comparable results in the same animals throughout time and between animals. In other words, the phase space used to define sleep states must be stable. This phase space was constructed so that the separation between wake and sleep on the one hand and REM and NREM on the other hand used orthogonal axis. This simple space is remarkably consistent among animals and across days as can be seen by the similar position of the clouds of points representing each state (Figure 5A).

We first quantified this similarity in the same animals between days and between light and dark cycles. We used the thresholds defined for one animal on a given light-cycle to score test data from the same animal on a subsequent light- or dark-cycle. The scoring was then compared with that obtained using thresholds determined from the test data itself. Thresholds for one animal were calculated as the distance from the SWS peak, both for OB gamma activity and HPC theta/delta ratio, to correct for the shifts in overall amplitude that might be caused for instance by changes in recording site (see methods for details).

We found that the observed consistency was sufficient to perform highly accurate scoring on the next day light cycle (average over recordings: 97 ± 0.5%, Cohen's K: 0.97, n=15, Figure 5Bi) and during the dark cycle (average over recordings: 96 ± 0.9%, Cohen's K: 0.94, n=4, Figure 5Bii) using independently defined thresholds (see methods).

We next compared the phase space used for sleep scoring between animals. We found that after normalizing distributions to the mean NREM values, both OB and HPC distributions were highly reproducible across mice and the independently determined thresholds had very close values (Figure 5C). Scoring one animal using the thresholds determined for another as above, we found that scoring was also highly reliable (average over recordings: 90 ± 2.5%, Cohen's K: 0.85, n=15, Figure 5D).

Finally, since gamma oscillations in the olfactory bulb have been linked with information processing and novelty (Kay *et al.*, 2009), we exposed 8 mice to a novel environment for 15min, during which the animals actively explored. On average only 2 ± 1.1% of the time was misclassified as sleep. This demonstrates that any changes in gamma activity linked to behaviour remain well within the bounds of the wake state as previously defined.

This demonstrates that brain state related changes in gamma power are quantitatively robust over multiple days, throughout the circadian cycle and during exposure to new environment. Moreover the phase space thus constructed is highly reproducible between animals. This makes it an excellent parameter to use for automatic methods of scoring and a promising tool for comparing sleep in cohorts of animals.

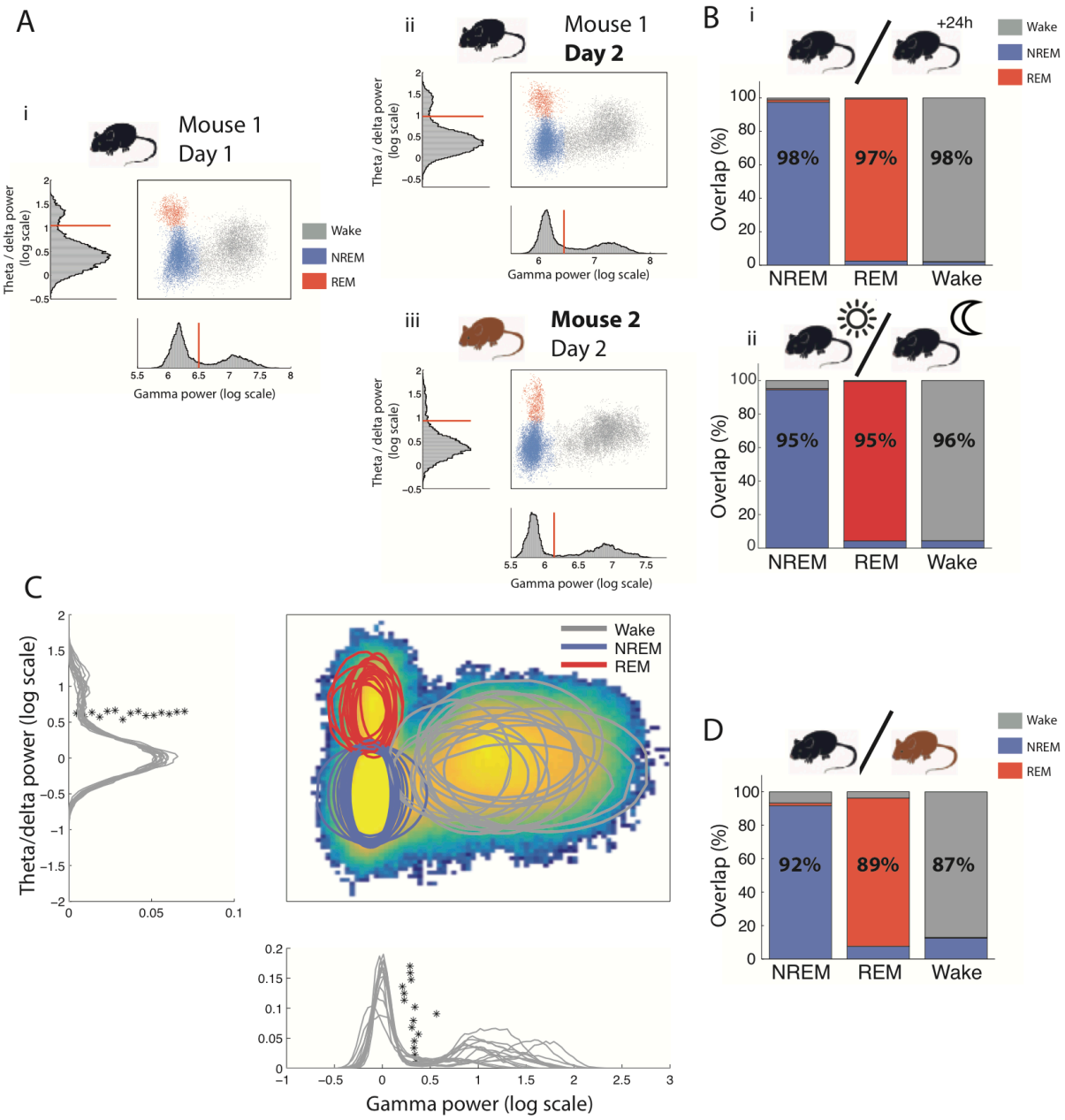

248

249

Figure 5

A. *Phase space of brain states and corresponding histograms along the relevant axis with automatically determined thresholds of the same mouse over different days (i vs ii) and in two different mice (i vs iii) demonstrating the highly conserved architecture across time and individuals.*

B. *Overlap of scoring using thresholds determined on the same mouse on one day and applied the following day (i) and during successive light and dark periods (ii). Each column gives the percent of the brain state (x label) identified using thresholds determined on the reference data set that is classified as NREM (blue), REM (red) and wake (grey) using thresholds determined using data from different days (i) or during the light period (ii). (n=10 mice were recorded on consecutive days and used for inter-day scoring, n=5 mice were recorded over a 24h period of light and dark periods)*

C. *Heat map of point density averaged over all phase spaces for all mice (n=15). Circles show the 95% boundaries of NREM, REM and wake for each mouse. Histograms from all mice are shown along the relevant axis with automatically determined thresholds (*).*

D. *Overlap of scoring using thresholds determined on one mouse and applied to a different mouse (n=15 mice). As in B.*

250

A powerful tool to study mismatch between brain state and motor activity

A major issue with current approaches to sleep scoring is that EMG activity conflates absence of movement and sleep which suffers from notable exceptions such as during freezing behaviour. Freezing is a widely-studied behaviour in paradigms such as fear conditioning. It is defined as a complete absence of all movement except for respiration. This absence of movement is associated with a strong drop in EMG power. Although it has been shown that average EMG power is lower during sleep than freezing (Steenland & Zhuo, 2009), we investigated whether freezing could be misclassified as sleep using EMG power and whether OB gamma power could resolve this issue. Six mice were therefore fear-conditioned by pairing tones with mild footshocks and during test sessions displayed robust freezing to tone presentation (see methods).

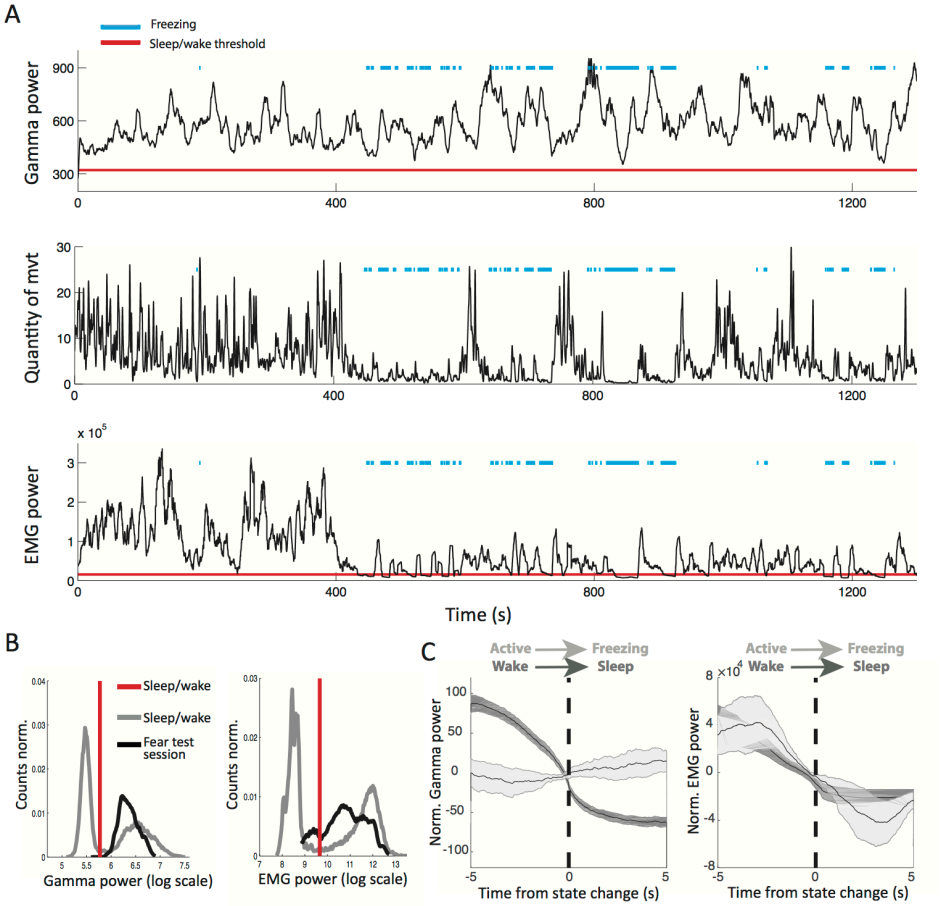

Figure 6

A. *OB gamma power, quantity of movement and EMG power during an example test session during which the mouse displayed freezing episodes (blue line). Freezing was determined using the quantity of movement. Red lines indicate the sleep/wake thresholds independently determined during a previous session in the homecage for OB gamma and EMG power.*

B. *In gray, distribution of gamma (left) and EMG (right) power during the homecage session. In black the distribution during the test session, including the freezing periods. For gamma power all values recorded during the test session are classified as wake whereas the EMG power during values from freezing periods are below the threshold.*

C. *Averaged OB gamma power (left) and EMG power (right) triggered on two types of transitions from mobility to immobility: the wake to sleep transition and the active to freezing transition. OB gamma power drops when the animal falls asleep but not when the animal freezes. EMG power shows similar changes during freezing and sleep onset (n=6, error bars : s.e.m)*

The example session shown in figure 6A illustrates the strong expected drop in EMG power during freezing periods, sometimes below the sleep/wake threshold independently determined during a previous sleep session. Although the EMG power is indeed on average higher than during the sleep state, freezing time point can be misclassified as sleep (Figure 6B). In the example in figure 6A, 54% of freezing periods were classified as sleep and EMG shows a similar drop in power at freezing and sleep onset (Figure 6C). In sharp contrast, gamma power remains systematically above the sleep/wake threshold (Figure 6B). Gamma power triggered on freezing onset shows that the variable is independent of freezing onset (Figure 6C).

Freezing is a behaviour that dissociates complete immobility from sleep, allowing us to clearly show that OB gamma power is tracking transitions from wake to sleep and not from mobility to immobility. EMG in contrast is an unreliable marker for sleep scoring when animals are susceptible to display immobility during wakefulness.

Olfactory bulb activity is tightly linked to REM/NREM state

The OB receives input from multiple neuromodulatory systems (see discussion) and it may therefore be a reliable marker of brain states in general. We therefore investigated whether OB activity changed between REM and NREM sleep. The results presented figure 1B shows that during REM sleep there is a drop of power in the 10-30Hz beta band. This rhythm has been shown to be modulated by learning (Beshel *et al.*, 2007; Martin & Ravel, 2014) but not previously related to vigilance states.

Comparing OB and HPC spectrograms, a loss of synchrony in the beta band is visible in the OB, tightly locked to the appearance of the theta band in the HPC for each bout of REM sleep (Figure 7A). We found a high correlation between HPC theta/delta power and OB beta power, with most time points clearly segregating into two clusters (Figure 7B). The distribution of power in the 10-15Hz band during sleep for all mice shows a spike and slab structure similar to that observed for the theta/delta ratio in the HPC (Figure 7C). This allows us to classify brain states into a high-beta and a low-beta state and evaluate to what extent they correspond with NREM and REM periods.

We compared the OB-based scoring with that obtained using HPC activity. We quantified both the sensitivity and specificity of the method, sensibility being defined as the proportion of classical HPC-based REM correctly identified as REM, and specificity being defined as the proportion of 'true' or HPC-based NREM correctly identified as NREM (Figure 7D). This shows that OB drops in beta power is highly specific to REM but misses around 25% of 'true' REM periods. Altogether, these results demonstrate a striking relationship between OB oscillations and brain states.

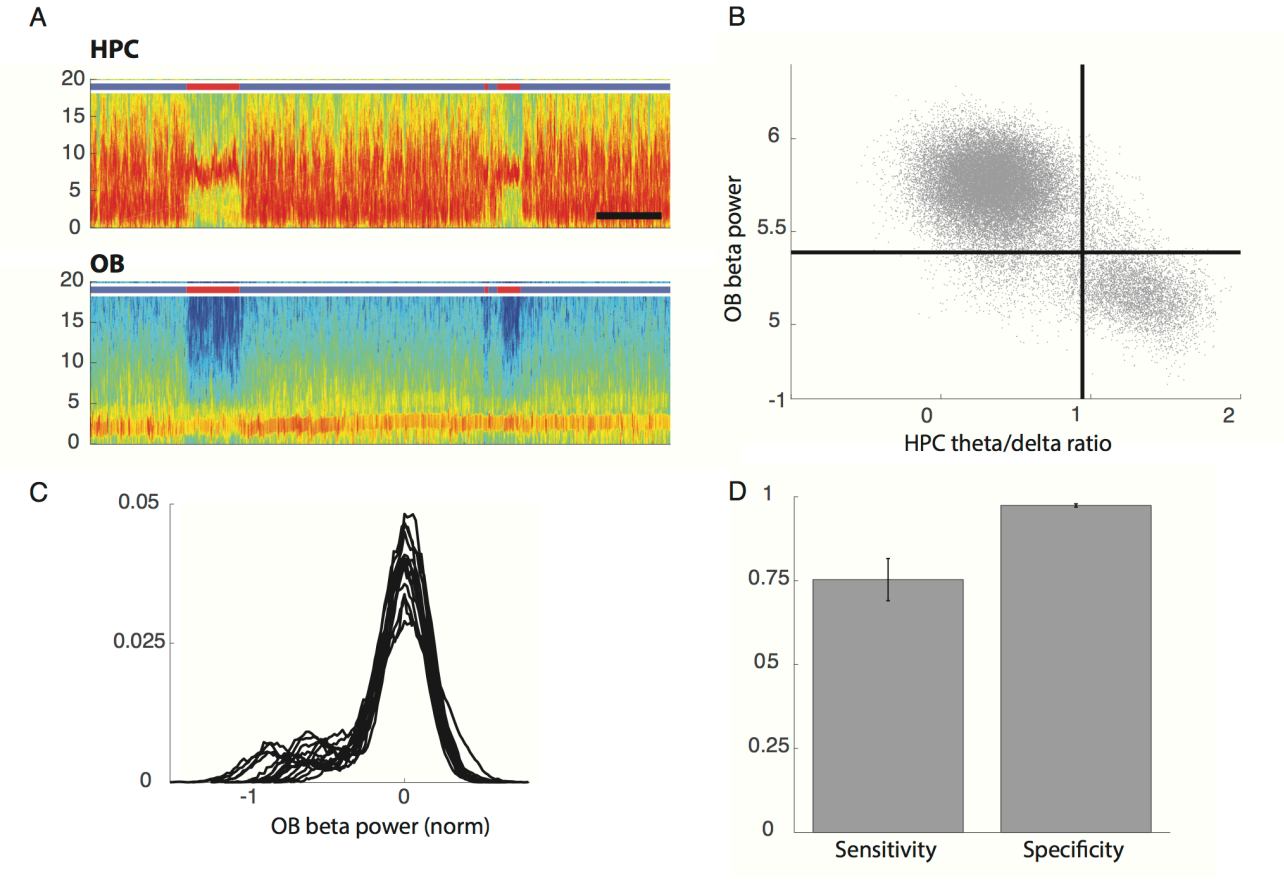

Figure 7

A. *Example spectrograms of OB (top) and HPC (bottom) activity. The coloured bar indicates the state of the animal defined using OB and HPC activity: blue for SWS, red from REM and gray for wake. Note that during REM periods, defined by strong theta activity in the HPC, there is a drop in a wide band from 10 to 20Hz in the OB. (bar : 3min)*

B. *Correlation of OB beta power and HPC theta/delta ratio power for the same mouse as in A with automatically determined thresholds for each distribution in black. Dots in the upper left and lower right hand corner are identically classified by both approaches.*

C. *Distributions of beta power in the OB during sleep (n=15).*

D. *Sensitivity and specificity of REM identification using OB beta power, where true REM is defined using the HPC activity. Sensitivity is defined as the proportion of 'true' or HPCal REM correctly identified as REM and specificity as the proportion of 'true' or HPCal SWS correctly identified as SWS. (n=15, error bars : s.e.m)*

Discussion

Here we show that automatic sleep scoring can be achieved with brain signals only. We found that gamma oscillations in the olfactory bulb was a brain signal usable to continuously identify the different sleep stages. It can be substituted to the muscular activity or body movements that are required in all the other sleep scoring methods.

Utility of the novel method

The novel sleep scoring method we propose here relies on activity recorded in the HPC and the OB only. Implantation of electrodes for recording LFP in these two areas is easy to achieve because both areas show robust oscillations in the theta and gamma ranges respectively at multiple recording sites. After implantation the method is full automated and therefore

312 removes the time-consuming steps of scoring by hand the full data set or a training set to
313 calibrate semi-automatic algorithms. We have shown that this method for sleep scoring is
314 robust to slight changes in implantation site, across days and between different animals. It
315 therefore allows easy comparison between mice and throughout time, and may be between
316 data sets from different laboratories.

317 Beyond the technical ease of use, this method also provides a promising framework for the
318 study of the dynamics of brain states. Using activity recorded in the brain and not muscle
319 activity allows to track sleep/wake activity independently of movement. This could provide the
320 heretofore lacking methodology to study phenomena such as REM without atonia induced in
321 lesion studies (Lu *et al.*, 2006). Our construction of a highly-reproducible phase space across
322 animals and days allows for easy pooling of data sets and comparison of dynamics. Finally,
323 gamma activity in the OB is a variable with fast dynamics that allows to study fine time-scale
324 transitions not accessible to other, slower sleep-related oscillations such as delta power.

325 ***The olfactory bulb gamma oscillations as a gating mechanisms during sleep***

326 Interestingly, olfaction is the only sensory system in the mammalian brain that does not pass
327 through the thalamic relay before reaching the cortex. The thalamus is thought to play an
328 important role in gating (McCormick & Bal, 1994) during sleep.

329 This naturally raises the question as to where state-dependent gating occurs along the
330 olfactory pathway. Part of the gating could occur in the piriform cortex. Indeed, during
331 anesthesia different states can coexist with wake-like and sleep-like periods that display slow
332 membrane oscillations comparable to up and down states (Murakami *et al.*, 2005).
333 Interestingly, suppression of sensory response is observed in the piriform cortex but not in the
334 OB since during sleep-like states (Murakami *et al.*, 2005). These results have to be taken with
335 caution since sensory response in anesthetized preparations are poorly predictive of responses
336 in natural situation without drug (Cotillon-williams & Edeline, 2002).

337 However, we show here that gamma oscillations could also serve participate in this gating.
338 Gamma oscillations are thought to play an important role in information transmission
339 throughout the brain (Buzsáki & Wang, 2012). In particular, in the OB they are hypothesized to
340 play an essential role for effective transmission and processing of odour input to the piriform
341 and orbitofrontal cortices (Mori *et al.*, 2013). Indeed, gamma oscillations are influenced by task
342 demands (Beshel *et al.*, 2007; Martin & Ravel, 2014) and their suppression impairs sensory
343 processing (Lepousez & Lledo, 2013). Therefore, the suppression of gamma oscillations during
344 sleep could provide another mechanism for sensory gating, the lack of synchronous firing
345 among OB neurons rendering inefficient the transfer of information to secondary olfactory
346 areas. Moreover, the decrease in OB gamma power is observed in SWS and REM sleep as well
347 and could explain the lack of response in all sleep states. Interestingly, gamma oscillations are
348 strongly reduced during anaesthesia, further supporting their possible link with states of
349 suppressed sensory input (Chery *et al.*, 2014).

350 ***The olfactory bulb as a marker for brain states***

351 Altogether, these observations raise the question as to why, compared with other areas, the
352 OB is so well suited to identifying the switch between sleep and wakefulness. One explanation
353 comes from the fact that the olfactory bulb receives massive projections from most of the
354 neuromodulator systems and notably those involved in the control of sleep/wake alternation.

355 For instance, the OB receives large projection from the cholinergic nuclei and expresses high
356 level of cholinergic receptors (D'Souza & Vijayaraghavan, 2014). Accordingly, acetylcholine has
357 been proposed as a neuromodulator that could enable sensory gating in the olfactory system

(Mori *et al.*, 2013). However, given the roughly similar reduction of gamma power in both REM and NREM periods and the high cholinergic levels during REM, this neuromodulator seems an unlikely candidate for gamma suppression during sleep.

In addition to cholinergic innervation of the OB, other neuromodulatry systems know to be involved in sleep regulation send projection to the OB. Hypocretinergic/orexinergic projections from the hypothalamus sparsely innervate all of the layers of the OB (Gascuel *et al.*, 2012) and the locus coeruleus sends extremely dense noradrenergic projection to the OB that are 10 times greater than to any other part of the cerebral cortex (Shipley *et al.*, 1985). Moreover, receptors of both neuromodulatory systems are strongly expressed in the OB (McCune *et al.*, 1993; Hardy *et al.*, 2005). Since these neuromodulators have an essential role in regulation of the sleep/wake cycle and have been show to enhance gamma oscillations in the OB or in other systems (Hall & Delaney, 2001; Gire & Schoppa, 2008; Li & Cleland, 2013; Ishibashi *et al.*, 2015), they are potential candidates for the state switching we observe in the OB.

A recent method has been proposed to track continuously vigilance states by tracking pupil diameter (McGinley *et al.*, 2015). Interestingly it was showed that pupil fluctuation follows the activity of cholinergic and adrenergic activity in the cortex (Reimer *et al.*, 2016). However, this method is difficult to implement in freely moving animals. The results showed here suggest that the gamma power of the olfactory bulb could offer an attractive strategy for the monitoring of vigilance states in natural situations. Of course, the question of whether OB could have an influence on sleep/wake alternation will deserve further investigation.

Nevertheless, we show that OB gamma oscillations can be used as a direct read-out of the brain network responsible for sleep/wakefulness cycles that constitutes the first method allowing a clear identification of sleep and wake states with brain signal only.

Materials and methods

Subjects and surgery

A total of 15 C57Bl6 male mice (*Mus musculus*), 3–6 months old, were implanted with electrodes (tungsten wires) in the right olfactory bulb (AP +4, ML +0.5, DV −1.5) and in the right CA1 hippocampal layer (AP -2.2, ML +2.0, DV −1.0). 6 of these mice were also implanted with a hooked EMG wire in the right nuchal muscle. 6 mice were also implanted in the right prefrontal cortex (AP +2.1, ML +0.5, DV −0.5) and parietal cortex (AP -1.7, ML +1.0, DV −0.8). One mouse was recorded with a sixteen-site linear probe (100um spacing, Neuronexus Tech, Ann Arbor, MI, USA). During recovery from surgery (minimum 3 d) and during all experiments, mice received food and water ad libitum. Mice were housed in an animal facility (08:00–20:00 light), one per cage after surgery. All behavioural experiments were performed in accordance with the official European guidelines for the care and use of laboratory animals (86/609/EEC) and in accordance with the Policies of the French Committee of Ethics (Decrees n° 87–848 and n° 2001–464). Animal housing facility of the laboratory where experiments were made is fully accredited by the French Direction of Veterinary Services (B-75-05- 24, 18 May 2010). Animal surgeries and experimentations were authorized by the French Direction of Veterinary Services for K.B. (14-43).

Signals from all electrodes were recorded using an Intan Technologies amplifier chip (RHD2216, sampling rate 20 KHz). Local field potentials were sampled and stored at 1,250 Hz. Analyses were performed with custom made Matlab programs, based on generic code that can be downloaded at http://www.battaglia.nl/computing/ and http://fmatoolbox.sourceforge.net/.

Fear conditioning

Habituation and fear conditioning took place in context A consisting of a square transparent Plexiglas box in a black environment with a shock grid floor and cleaned with ethanol (70%) before and after each session. Extinction learning and test sessions were performed in context B consisting of cylindrical transparent Plexiglas walls with a grey plastic floor placed in a white environment and cleaned with acetic acid (1%) before and after each session.
To score freezing behaviour animals were tracked using a home-made automatic tracking system that calculated the instantaneous position of the animal and the quantity of movement defined as the pixel-wise difference between two consecutive frames. The animals were considered to be freezing if the quantity of movement was below a manually-set threshold for at least 2 s.
On day 1, mice were submitted to a habituation session in context A, in which they received four presentations of the CS- and of the CS+ (total CS duration, 30 s; consisting of 50-ms pips at 0.9 Hz repeated 27 times, 2 ms rise and fall; pip frequency, 7.5 kHz or white-noise, 80 dB sound pressure level). Discriminative fear conditioning was performed on the same day by pairing the CS+ with a US (1-s foot-shock, 0.6 mA, 8 CS+ US pairings; inter-trial intervals, 20–180 s). The onset of the US coincided with the offset of the CS+. The CS- was presented after each CS+ US association but was never reinforced (5 CS- presentations; inter-trial intervals, 20–180 s). On day 2 and day 3, conditioned mice were submitted to a test session in context B during which they received 4 and 12 presentations of the CS- and CS+, respectively.

Histological analysis

After completion of the experiments, mice were deeply anesthetized with ketamine/xylazine solution (10% /1%). With the electrodes left *in situ*, the animals were perfused transcardially with saline (~50 ml), followed by ~50 ml of PFA (4 g/100 mL). Brains were extracted and placed in PFA for postfixation for 24 h, transferred to PBS for at least 48 h, and then cut into 50-µm-thick sections using a freezing microtome and mounted and stained with hard set vectashield mounting medium with DAPI (Vectorlabs).

Bimodality quantification

Bimodality was quantified by fitting a mixture of two normal distributions and evaluating either Ashman's D (Ashman *et al.*, 1994), $D = \sqrt{2}\frac{|\mu_1-\mu_2|}{|\sigma_1+\sigma_2|}$ where D>2 is required for a clean separation or the overlap of the two distributions.

Automatic sleep scoring algorithm

LFP recordings from the OB were filtered in the gamma (50-70Hz) band and instantaneous amplitude derived from the Hilbert Transform. This time-series was then smoothed using a 3s sliding (Fig.1D) window and the distribution of values could be fit with a mixture of two normal distributions. To maximize the probability of correct classification, the threshold between sleep and wake should be defined as the intersection of these two distributions. This value however depends on the amplitude of the two distributions and therefore on the ratio of sleep and wake recorded. To establish a threshold independent of this ratio, the two distributions are normalized to each have area one (Fig2.Bi, right) and the intersection of these distributions is used. Values inferior to this value are classified as sleep and those superior as wake. Periods of sleep and wake shorter than 3s were merged into the surrounding periods to avoid artificially short epochs. Then, LFP recordings from the HPC restricted to the sleep periods defined above, were filtered in the theta (5-10Hz) and delta (2-5Hz) bands and instantaneous amplitude derived from the Hilbert Transform. The ratio of the theta and delta powers was smoothed using a 2s sliding window and the distribution of values was fit by a single normal distribution that accounted for the NREM data points (low theta/delta ratio). The REM/NREM threshold was placed at the point above which the residuals systematically explained more than 50% of the actual data (Fig2.Bii). Periods of NREM and REM shorter than 3s were merged into the surrounding periods to avoid artificially short epochs.

Automatic EMG scoring

Automatic EMG scoring was performed in a similar fashion to automatic OB gamma power scoring. EMG data was filtered in the 50-300Hz band and instantaneous amplitude derived from the Hilbert Transform. This time-series was then smoothed using a 2s sliding window and the distribution of values could be fit with a mixture of two normal distributions. The intersection of these two distributions, once normalized provided the sleep-wake threshold. The theta/delta power ratio and period dropping procedures are the same as above.

Manual sleep scoring

Automatic scoring was performed independently by two experimenters using a home-made matlab GUI. The scorers were provided with EMG (raw, filtered in the 50-300Hz band and smoothed instantaneous amplitude) and HPC (raw, low frequency spectrogram and smoothed instantaneous theta to delta ratio) and 3s windows were determined to be NREM, REM or Wake depending on which brain state was judged to be in the majority.

Evaluation of overlap of scoring methods

The percentage agreement between methods is calculated for each state and shown in the relevant figures. Given that average agreement can be potentially misleading, we also used the confusion matrix to calculate Cohen's κ (Cohen, 1960) defined as :

$$K = \frac{P_o - P_e}{1 - P_e}$$

with

$P_o = \sum_{i=1}^{3} p_{ii}$ where p_{ii} is the probability that both methods classify data as the identical state i (REM, NREM, wake).

$P_e = \sum_{i=1}^{3} p_{1i} \times p_{2i}$ where p_{1i} and p_{2i} are the independent probabilities that methods 1 and 2 will classify data as state i.

We applied the same criteria as used in (Libourel *et al.*, 2015) to evaluate the quality of the agreement :

Quality of agreement	Cohen's κ
Almost perfect	>0.81
Substantial	0.8-0.61
Moderate	0.6-0.41
Fair	0.4-0.21
Slight	0.2-0
Poor	<0

Acknowledgements

S.B. did the experiments and analyzed the data. M.M.L., G.d.L. and J.M.L. did several experiments included in the dataset. H.G. performed the histology. S.B. and K.B. wrote the manuscript with the help of M.M.L and J.M.L.. This work was supported by the Fondation pour la Recherche sur le Cerveau (FRC), by the French National Agency for Research ANR-12-BSV4-0013-02 (AstroSleep), by the CNRS: ATIP-Avenir (2014) and by the city of Paris (Grant Emergence 2014). This work also received support under the program Investissements d'Avenir launched by the French Government and implemented by the ANR, with the references: ANR-10-LABX-54 MEMO LIFE and ANR-11-IDEX-0001-02 PSL* Research University. G.d.L. and M.M.L. were funded by the Ministère de l'Enseignement Supérieur et de la Recherche, France. S.B. was funded by the ENS-Ulm, PSL Research University and the Ministère de l'Enseignement Supérieur et de la Recherche, France.

Competing interests

No conflicts of interest, financial or otherwise are declared by the authors.

References

Ashman, K.A., Bird, C.M., & Zepf, S.E. (1994) Detecting bimodality in astronomical datasets. *Astron. J.*, **108**, 2348.

Benington, J.H. & Heller, H.C. (1995) Restoration of brain energy metabolism as the function of sleep. *Prog. Neurobiol.*, **45**, 347–360.

Beshel, J., Kopell, N.J., & Kay, L.M. (2007) Olfactory bulb gamma oscillations are enhanced with task demands. *J. Neurosci.*, **27**, 8358–8365.

Brankack, J., Kukushka, V.I., Vyssotski, A.L., & Draguhn, A. (2010) EEG gamma frequency and sleep-wake scoring in mice: comparing two types of supervised classifiers. *Brain Res.*, **1322**, 59–71.

Buzsáki, G. & Wang, X.-J. (2012) Mechanisms of gamma oscillations. *Annu. Rev. Neurosci.*, **35**, 203–225.

Chery, R., Gurden, H., & Martin, C. (2014) Anesthetic regimes modulate the temporal dynamics of local field potential in the mouse olfactory bulb. *J. Neurophysiol.*, **111**, 908–917.

Chou, C.-H., Kuo, C.-C., Yu, Z.-E., Tai, H.-P., & Chen, K.-W. (2013) Extracting the Critical Frequency Bands to Classify Vigilance States of Rats by Using a Novel Feature Selection Algorithm. *Int. J. Comput. Commun. Eng.*, **2**, 277–280.

Cirelli, C. & Tononi, G. (2000) Gene expression in the brain across the sleep–waking cycle. *Brain Res.*, **885**, 303–321.

Cohen, J. (1960) A coefficientof agreement for nominal scales. *Educ. Psychol. Meas.*, **20**, 37–46.

Cotillon-williams, N. & Edeline, J. (2002) Evoked Oscillations in the Thalamo-Cortical Auditory System Are Present in Anesthetized but not in Unanesthetized Rats. *J. Neurophysiol.*, **89**, 1968–1984.

Crisler, S., Morrissey, M.J., Anch, a M., & Barnett, D.W. (2008) Sleep-stage scoring in the rat using a support vector machine. *J. Neurosci. Methods*, **168**, 524–534.

D'Souza, R.D. & Vijayaraghavan, S. (2014) Paying attention to smell: Cholinergic signaling in the olfactory bulb. *Front. Synaptic Neurosci.*, **6**, 1–11.

Datta, S. & Hobson, J.A. (2000) The rat as an experimental model for sleep neurophysiology. *Behav. Neurosci.*, **114**, 1239–1244.

Gascuel, J., Lemoine, A., Rigault, C., Datiche, F., Benani, A., Penicaud, L., & Lopez-Mascaraque, L. (2012) Hypothalamus-olfactory system crosstalk: orexin a immunostaining in mice. *Front. Neuroanat.*, **6**, 44.

Gervasoni, D., Lin, S., Ribeiro, S.T., Soares, E.S., Pantoja, J., & Nicolelis, M.A.L. (2004) Global Forebrain Dynamics Predict Rat Behavioral States and Their Transitions. *J. Neurosci.*, **24**, 11137–11147.

Gire, D.H. & Schoppa, N.E. (2008) Long-term enhancement of synchronized oscillations by adrenergic receptor activation in the olfactory bulb. *J. Neurophysiol.*, **99**, 2021–2025.

552 Gross, B. a, Walsh, C.M., Turakhia, A. a, Booth, V., Mashour, G. a, & Poe, G.R. (2009) Open-
553 source logic-based automated sleep scoring software using electrophysiological
554 recordings in rats. *J. Neurosci. Methods*, **184**, 10–18.

555 Hall, B. & Delaney, K. (2001) Cholinergic Modulation of Odor-Evoked Oscillations in the Frog
556 Olfactory Bulb. *Biol. Bull.*, **201**, 276–277.

557 Hardy, A.B., Aïoun, J., Baly, C., Julliard, K. a, Caillol, M., Salesse, R., & Duchamp-Viret, P. (2005)
558 Orexin A modulates mitral cell activity in the rat olfactory bulb: patch-clamp study on
559 slices and immunocytochemical localization of orexin receptors. *Endocrinology*, **146**,
560 4042–4053.

561 Iber, C., Ancoli-Israel, S., Chesson, A., Quan, S.F., & Medecine, for the A.A. of S. (2007) *The*
562 *AASM Manual for the Scoring of Sleep and Associated Events: Rules, Terminology, and*
563 *Technical Specification*, 1st edn. American Academy of Sleep Medecine, Westchester,
564 Ilinois.

565 Imeri, L. & Opp, M.R. (2009) How (and why) the immune system makes us sleep. *Nat. Rev.*
566 *Neurosci.*, **10**, 199–210.

567 Ishibashi, M., Gumenchuk, I., Kang, B., Steger, C., Lynn, E., Molina, N.E., Eisenberg, L.M., &
568 Leonard, C.S. (2015) Orexin Receptor Activation Generates Gamma Band Input to
569 Cholinergic and Serotonergic Arousal System Neurons and Drives an Intrinsic Ca(2+)-
570 Dependent Resonance in LDT and PPT Cholinergic Neurons. *Front. Neurol.*, **6**, 120.

571 Kay, L.M., Beshel, J., Brea, J., Martin, C., Rojas-Líbano, D., & Kopell, N.J. (2009) Olfactory
572 oscillations: the what, how and what for. *Trends Neurosci.*, **32**, 207–214.

573 Lepousez, G. & Lledo, P.-M. (2013) Odor discrimination requires proper olfactory fast
574 oscillations in awake mice. *Neuron*, **80**, 1010–1024.

575 Li, G. & Cleland, T.A. (2013) A Two-Layer Biophysical Model of Cholinergic Neuromodulation
576 in Olfactory Bulb. *J. Neurosci.*, **33**, 3037–3058.

577 Liang, S.F., Kuo, C.E., Hu, Y.H., & Cheng, Y.S. (2012) A rule-based automatic sleep staging
578 method. *J. Neurosci. Methods*, **205**, 169–176.

579 Libourel, P.-A., Corneyllie, A., Luppi, P.-H., Chouvet, G., & Gervasoni, D. (2015) Unsupervised
580 online classifier in sleep scoring for sleep deprivation studies. *Sleep*, **38**, 815–828.

581 Louis, R.P., Lee, J., & Stephenson, R. (2004) Design and validation of a computer-based sleep-
582 scoring algorithm. *J. Neurosci. Methods*, **133**, 71–80.

583 Lu, J., Sherman, D., Devor, M., & Saper, C.B. (2006) A putative flip–flop switch for control of
584 REM sleep. *Nature*, **441**, 589–594.

585 Manabe, H. & Mori, K. (2013) Sniff rhythm-paced fast and slow gamma-oscillations in the
586 olfactory bulb: relation to tufted and mitral cells and behavioral states. *J. Neurophysiol.*,
587 **110**, 1593–1599.

588 Martin, C. & Ravel, N. (2014) Beta and gamma oscillatory activities associated with olfactory
589 memory tasks: different rhythms for different functional networks? *Front. Behav.*
590 *Neurosci.*, **8**, 218.

591 McCormick, D.A. & Bal, T. (1994) Sensory gating mechanisms of the thalamus. *Curr. Opin.*
592 *Neurobiol.*, **4**, 550–556.

McCune, S.K., Voigt, M.M., & Hill, J.M. (1993) Expression of multiple alpha adrenergic receptor subtype messenger RNAs in the adult rat brain. *Neuroscience*, **57**, 143–151.

McGinley, M.J., Vinck, M., Reimer, J., Batista-brito, R., Zagha, E., Cadwell, C.R., Tolias, A.S., Cardin, J.A., & Mccormick, D.A. (2015) Waking State : Rapid Variations Modulate Neural and Behavioral Responses. *Neuron*, **87**, 1143–1161.

Mori, K., Manabe, H., Narikiyo, K., & Onisawa, N. (2013) Olfactory consciousness and gamma oscillation couplings across the olfactory bulb, olfactory cortex, and orbitofrontal cortex. *Front. Psychol.*, **4**, 743.

Murakami, M., Kashiwadani, H., Kirino, Y., & Mori, K. (2005) State-Dependent Sensory Gating in Olfactory Cortex. *Neuron*, **46**, 285–296.

Rechtschaffen, A. & Kales, A. (1968) *A Manual of Standardized Terminology, Techniques and Scoring System of Sleep Stages in Human Subjects*. Brain Information Service/Brain Research Institute, University of California, Los Angeles.

Reimer, J., McGinley, M.J., Liu, Y., Rodenkirch, C., Wang, Q., McCormick, D.A., & Tolias, A.S. (2016) Pupil fluctuations track rapid changes in adrenergic and cholinergic activity in cortex. *Nat. Commun.*, **7**, 13289.

Rytkönen, K.-M., Zitting, J., & Porkka-Heiskanen, T. (2011) Automated sleep scoring in rats and mice using the naive Bayes classifier. *J. Neurosci. Methods*, **202**, 60–64.

Schenck, C.H. & Mahowald, M.W. (2002) REM sleep behavior disorder: clinical, developmental, and neuroscience perspectives 16 years after its formal identification in SLEEP. *Sleep*, **25**, 120–138.

Senut, M.C., Menetrey, D., & Lamour, Y. (1989) Cholinergic and peptidergic projections from the medial septum and the nucleus of the diagonal band of Broca to dorsal hippocampus, cingulate cortex and olfactory bulb: a combined wheatgerm agglutinin-apohorseradish peroxidase-gold immunohistochemical stu. *Neuroscience*, **30**, 385–403.

Shipley, M.T., Halloran, F.J., & de la Torre, J. (1985) Surprisingly rich projection from locus coeruleus to the olfactory bulb in the rat. *Brain Res.*, **329**, 294–299.

Steenland, H.W. & Zhuo, M. (2009) Neck electromyography is an effective measure of fear behavior. *J. Neurosci. Methods*, **177**, 355–360.

Stephenson, R., Caron, A.M., Cassel, D.B., & Kostela, J.C. (2009) Automated analysis of sleep-wake state in rats. *J. Neurosci. Methods*, **184**, 263–274.

Steriade, M., McCormick, D.A., & Sejnowski, T.J. (1993) Thalamocortical oscilations in the sleeping and aroused brain. *Science*, **262**, 679–685.

Veasey, S.C., Valladares, O., Fenik, P., Kapfhamer, D., Sanford, L.D., Benington, J.H., & Bucan, M. (2000) An automated system for recording and analysis of sleep in mice. *Sleep*, **23**, 1025–1040.

Wenk, H., Bigl, V., & Meyer, U. (1980) Cholinergic projections from magnocellular nuclei of the basal forebrain to cortical areas in rats. *Brain Res. Rev.*, **2**, 295–316.

Xie, L., Kang, H., Xu, Q., Chen, M.J., Liao, Y., Thiyagarajan, M., O'Donnell, J., Christensen, D.J., Nicholson, C., Iliff, J.J., Takano, T., Deane, R., & Nedergaard, M. (2013) Sleep Drives Metabolite Clearance from the Adult Brain. *Science*, **342**, 373–377.

634 Yu, Z., Kuo, C., Chou, C., & Chang, F. (2009) A Machine Learning Approach to Classify Sleep
635 Stages of Rats. In *SSIP "09/MIV"09 Proceedings of the 9th WSEAS International Conference*
636 *on Signal, Speech and Image Processing*. pp. 120–125.

637 Zeng, T., Mott, C., Mollicone, D., & Sanford, L.D. (2012) Automated determination of
638 wakefulness and sleep in rats based on non-invasively acquired measures of movement
639 and respiratory activity. *J. Neurosci. Methods*, **204**, 276–287.

640

641